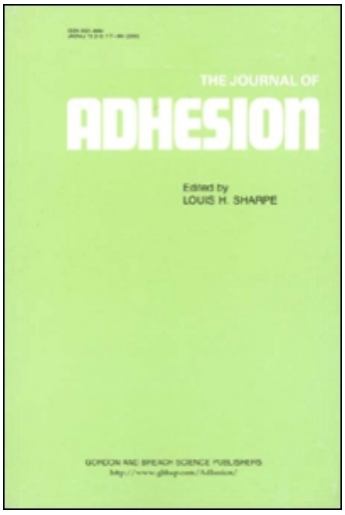

The Journal of Adhesion
Publication details, including instructions for authors and subscription information:
http://www.informaworld.com/smpp/title~content=t713453635

Crack Front Curvature in the Wedge Test

J. Jumel[a]; M. E. R. Shanahan[a]
[a] Université Bordeaux, Laboratoire de Mécanique Physique, CNRS UMR 5469, Talence, France

To cite this Article Jumel, J. and Shanahan, M. E. R.(2008) 'Crack Front Curvature in the Wedge Test', The Journal of Adhesion, 84: 9, 788 — 804
To link to this Article: DOI: 10.1080/00218460802352975
URL: http://dx.doi.org/10.1080/00218460802352975

The Journal of Adhesion, 84:788–804, 2008

ISSN: 0021-8464 print/1545-5823 online
DOI: 10.1080/00218460802352975

Taylor & Francis
Taylor & Francis Group

Crack Front Curvature in the Wedge Test

J. Jumel and M. E. R. Shanahan
Université Bordeaux, Laboratoire de Mécanique Physique, CNRS UMR 5469, Talence, France

The wedge test, as used for the evaluation of adhesive fracture energy, is usually considered to be a 2D geometry: its simple analysis implies independence of the width of the adhesive joint, b*. Recent work has shown this to be an over-simplification, at least in some circumstances, with (hypothesised) anticlastic bending giving rise to curvature of the crack front. As a result, crack front length,* a*, varies across the joint width leading to ambiguity in the interpretation of results to obtain fracture energy,* G_c*. This contribution constitutes a more detailed analysis of the geometry of the wedge test (in the particular case of one bending and one rigid substrate), treating the bent member as a plate, rather than as a simple beam. The Kirchhoff-Love plate theory is applied and solved by a perturbation method. Secondary curvature of the beam in the direction normal to the principal curvature results directly from the treatment, and this, in turn, leads to a concave crack front, corroborating the above-mentioned experimental observation.*

Keywords: 3D effect; Adhesion test; Crack front; Fracture energy; Wedge test

INTRODUCTION

The wedge, or cleavage, adhesion test is a useful method for the appraisal of adhesives, surface treatments, and structural bonding ageing properties. Two rectangular sheets of material are bonded together and a "wedge," inserted at one end of the structure in order to force apart the two adherends over a short initial distance. This leads to time-dependent separation in the remaining bonded region. Adhesion, or fracture, energy can be deduced as a function of separation rate, or crack speed. This technique has been exploited both experimentally and numerically. Examples are given in [1–11].

Received 7 May 2008; in final form 9 July 2008.
Address correspondence to M. E. R. Shanahan, Université Bordeaux 1, Laboratoire de Mécanique Physique, CNRS UMR 5469, 351 Cours de la Libération, 33405 Talence Cedex, France. E-mail: m.shanahan@lmp.u-bordeaux1.fr

With a judicious choice of adherend dimensions, the test permits one to remain in the domain of small strains behind the crack front, *i.e.,* in the separated zone, thus, limiting plastic deformation of the substrates, which could complicate analysis [10,11]. It can be used in the constant displacement mode (wedge position fixed with respect to the bonded joint), in the constant load mode (separation force maintained constant, therefore, akin to a double cantilever beam, DCB, although this latter generally uses rather thick adherends), or in the constant speed mode (in which the wedge is driven into the joint at a given rate) [11,12], although there is sometimes confusion about which analysis is relevant. We shall be principally interested in the constant displacement version in the following.

The purpose of this article is to consider the wedge test in three dimensions. The wedge test, as used for the evaluation of adhesive fracture energy, is usually considered to be in 2D geometry: its simple analysis implies independence of the width, b, of the adhesive joint. This assumption seems to be reasonably valid when the substrate (or *beam*) thickness is very small compared with the crack front width [13]. However, there is photographic evidence that this is an oversimplification of the situation in other cases [14–22]. As an example, Figure 1 shows the fracture of an essentially rigid substrate

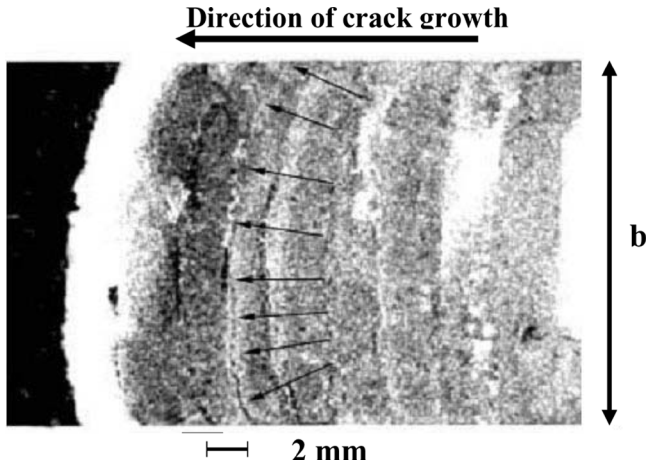

FIGURE 1 Example of curved crack front in wedge test observed by staining at different stages of fracture advance. Reprint from Figure 4 in Reference [23], S. Popineau, B. Gautier, P. Slangen and M. E. R. Shanahan, "A 3-D Effect in the Wedge Adhesion Test: Application of Speckle Interferometry", *J. Adhesion* **80** (12), 1173 (2004). http://www.informaworld.com

bonded to a more flexible beam, the overall joint width being b, as indicated. (This, in fact, corresponds to the case modelled below.) It can be seen that the crack front of this wedge test, viewed by staining the aluminium (rigid substrate)/epoxy/composite (flexible beam) joint at various stages of fracture progression, is clearly concave towards the direction of crack propagation [23]. (The slight asymmetry shown is not significant.) It may be noted in passing, that if environmental effects had been the cause, a *convex* crack front would have been observed. Other very distinct cases are shown in Chen *et al.* [19]. Although their work aims at a better understanding of the oscillation of crack paths over the adhesive thickness, this oscillatory behaviour can be seen to occur at curved crack fronts. This crack front curvature is often ignored, or dismissed as an "edge effect". There is, of course, a transition from plane strain near the joint middle to plane stress at the edges. However, in many cases, such as Figure 1, the effect is certainly more widespread than being confined to the edges, passing across the entire joint width, from $y = +b/2$ to $y = -\mathrm{b}/2$.

The effect shown in Figure 1 was studied in more detail using speckle interferometry [23]. Undoubtedly, a curvature effect was shown to be present and this was attributed to anticlastic bending [24] of the separated bending beam. Anticlastic bending is an effect due to opposite faces of a bent beam being in tension and in compression, leading to orthogonal compression and tension, respectively, due to Poisson's ratio. As a result, there is a tendency for inverse curvature normal to the principal bending curvature. A simple theory was developed which acceptably accounted for this curvature by introducing anticlastic bending in the far field. However, its major shortcoming was its inability to explain or predict the "competition" between the beam attempting to curve perpendicularly to the direction of primary bending under anticlastic effects, and the adhesive resistance near the crack front impeding separation. A numerical approach to this type of problem, assuming low ratios of joint thickness to length, and adhesive to adherend modulus, has also been recently reported [25].

The purpose of this article is to consider in some further detail phenomena related to a curved crack front and, although the general problem is exceedingly complicated, we present some progress towards its final solution. Using the principle of system evolution based on the fastest minimisation of the free (strain) energy of the bent, separated part(s) [or beam(s)] of the joint assembly, we show that the system will naturally adopt a curvature perpendicular to the principal one caused directly by the bending moment due to the wedge, and that this will lead to a curved crack front.

SIMPLE 2D ANALYSIS OF WEDGE TEST

We shall commence with a summary of the classic 2-dimensional (2D) analysis of the wedge test, as shown schematically in Figure 2. For simplicity, it is assumed that the lower adherend is completely rigid and that strain only occurs in the upper member. The system is taken to be a flexible upper *encastré* beam embedded in a "wall," the latter representing the zone which is still bonded. With the Cartesian coordinates (x, y, z) shown in Figure 2, the x and y axes are coplanar with the rigid substrate surface, and the origin is at the centre of the beam system at the position of application of bending load (the wedge end). We define $w(x)$ as the vertical displacement of the upper member with respect to the (x, y) plane, although there is no y dependence in this simple analysis. Applying the standard beam equation:

$$M(x) = EI\frac{d^2w}{dx^2}, \tag{1}$$

where $M(x)$ is the bending moment, here equal to Fx, F being the force acting upwards at the beam extremity, $x = 0$, E is Young's modulus of the beam, and I its second moment of inertia ($I = bh^3/12$ with b and h, respectively, width and thickness).

Equation (1) is solved with the boundary conditions of $w(a) = (dw/dx)(a) = 0$, leading to:

$$w(x) = \frac{F}{EI}\left(\frac{x^3}{6} - \frac{a^2x}{2} + \frac{a^3}{3}\right). \tag{2}$$

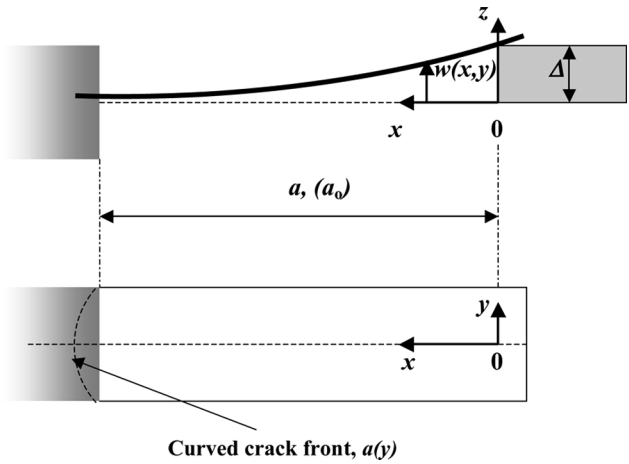

FIGURE 2 Schematic figure of wedge test treated as an *encastré* beam (top) separated from a rigid support [surface corresponding to (x, y) plane].

Using the fact that $w(0) = \Delta = Fa^3/3EI$, where Δ is the imposed vertical displacement of the flexed member at $x = 0$, allows us to simplify Equation (2) to give:

$$w(x) = \frac{\Delta}{2}\left[\frac{x}{a} - 1\right]^2\left[\frac{x}{a} + 2\right]. \tag{3}$$

The strain energy of the beam, U, is readily evaluated from:

$$U \approx \int_0^a \frac{M}{2} \cdot \frac{d^2w}{dx^2} \cdot dx = \frac{3EI\Delta^2}{2a^3}. \tag{4}$$

Application of the standard energy release rate equation (at fracture), in which G_c is fracture energy, principally in mode 1:

$$G_c + \frac{1}{b} \cdot \frac{\partial U}{\partial a} = 0, \tag{5}$$

corresponding to crack growth at the wall, or effective increase in length of the free beam, permits evaluation of the strain energy release rate, or energy of adhesion:

$$G_c = \frac{3E\Delta^2h^3}{8a^4}. \tag{6}$$

Equation (6) is the classic wedge test equation, in this case with a pre-factor of 3/8 since a simple beam is treated. (The more commonly used two flexible beam system has a pre-factor of 3/16.) Although a good approximation for narrow (or long) beams, with $a/b \gg 1$, note that, strictly, Equation (6) applies to conditions of plane stress, or alternatively Poisson's ratio, $\nu = 0$. If the joint width, b, is significant (or if the beam is short), a correction is already required to Equation (6). Instead of using a bending rigidity of EI [see Equation (1) or (4)], this term should be replaced by $EI\ (1 - \nu^2)$ [*cf.* Equation (7) and also Equation (16)] to allow for the frustrated tendency towards transverse bending [26,27]. With a plate material possessing a value of ν of *ca.* 0.3, this amounts to an increase of *ca.* 10%, which is not negligible. In the above, and what follows, we retain the symbol G_c, without specifying failure mode. There will be some mode mixity due to the asymmetry of this test, but failure will be mainly in mode 1.

Also note that effects of root rotation and deflection [28,29] are neglected here.

3D ANALYSIS OF SEPARATED ADHEREND (PLATE) AND CRACK FRONT

The main aim of this article is to suggest an improvement of the classical beam model for wedge test analysis taking into account crack front

curvature, using the classical hypothesis of an *encastré* beam in simple bending.

It is more realistic to treat the "beam" as a 3D object, or more specifically, as a "plate". In this case, we have potential variability of strains, displacements, and stresses along the y direction, where $-b/2 \leq y \leq +b/2$. It is then useful to introduce the *flexural rigidity* of the plate, D, as:

$$D = \frac{Eh^3}{12(1-\nu^2)}, \tag{7}$$

where ν is Poisson's ratio.

The basic equations describing bending behaviour are given by the Kirchhoff-Love plate theory. We define the free (elastic, strain) energy of the plate per unit surface in the (x, y) plane as $\delta^2 W$. The W refers to the total free energy in the 3D plate, and $\delta^2 W$, therefore, represents free energy surface *density*, which is twice integrated (over x and y) to give W. W is used here to differentiate it from the 2D beam case, where the symbol U was used, since w can now be a function of both x and y. Free energy density is related to the three curvature terms, $w_{xx} = \partial^2 w/\partial x^2$, $w_{yy} = \partial^2 w/\partial y^2$ and $w_{xy} = \partial^2 w/\partial x \partial y$ by the expression [30]:

$$\begin{aligned}\delta^2 W &= \frac{D}{2}\left[(w_{xx}+w_{yy})^2 - 2(1-\nu)(w_{xx}w_{yy} - w_{xy}^2)\right] \\ &= \frac{D}{2}\left[w_{xx}^2 + w_{yy}^2 + 2\nu w_{xx}w_{yy} + 2(1-\nu)w_{xy}^2\right].\end{aligned} \tag{8}$$

Values of w_{xx}, w_{yy}, and w_{xy} are required in Equation (8). An exact evaluation of these terms would be exceedingly difficult, but we approach the problem by assuming that the plate shape following coordinate x is essentially that corresponding to the standard 2D analysis briefly presented above [Equation (3)], but perturbed in the y direction by lateral bending effects. Anticipating the final result, the crack length, a, now becomes a function of y, that is: $a(y)$. It is convenient to introduce the notation, $X(x, y) = x/a(y)$. As a consequence, we can rewrite Equation (3) as:

$$w(x, y) = \frac{\Delta}{2}[X^3(x, y) - 3X(x,y) + 2]. \tag{9}$$

This, of course, amounts to relaxing the *encastré* constraint, or more precisely, assuming that the wall assumes a curvature in the (x, y) plane corresponding to the crack front shape being sought. As in the 2D case above, in the present analysis root rotation and deflection

[28,29] are neglected, although it is recognised that these effects are potentially important in the overall problem.

Evaluation of the various curvatures, w_{xx}, w_{yy}, and w_{xy}, using Equation (9) and insertion into Equation (8) is straightforward, if rather complicated, and leads to:

$$\begin{aligned}\delta^2 W(X,y) = \frac{9D\Delta^2}{8a(y)^4}\Bigg[&4X^2(1-2X^2)^2\left(\frac{\partial a}{\partial y}\right)^4 \\ &-2\left(\frac{\partial a(y)}{\partial y}\right)^2\left(-1+X^4(\nu-9)+2X^2(3-\nu)+\nu\right. \\ &+2X^2\left(1-3X^2+2X^4\right)\,a(y)\,\frac{\partial^2 a(y)}{\partial y^2}\Bigg) \\ &+X^2\Bigg(4+4\nu(1-X^2)\,a(y)\,\frac{\partial^2 a(y)}{\partial y^2} \\ &+(1-X^2)^2 a(y)^2\left(\frac{\partial^2 a(y)}{\partial y^2}\right)^2\Bigg)\Bigg]. \end{aligned} \tag{10}$$

The total elastic strain energy of the plate, W, is the integral of $\delta^2 W$ over the free surface of the plate and can be written:

$$W = \int_{-b/2}^{+b/2}\int_0^{a(y)} \delta^2 W dX\, dy. \tag{11}$$

Energy W is a minimum at equilibrium. The first integration, with respect to X, is again relatively easy, although unwieldy, and Equations (10) and (11) yield:

$$\begin{aligned}W = \int_{-b/2}^{+b/2}\Bigg[\frac{3D\Delta^2}{70a(y)^3}\Bigg[&35+11\left(\frac{\partial a(y)}{\partial y}\right)^4+14\nu a(y)\frac{\partial^2 a(y)}{\partial y^2} \\ &+2a^2(y)\left(\frac{\partial^2 a(y)}{\partial y^2}\right)^2-2\left(-21+14\nu+a(y)\frac{\partial^2 a(y)}{\partial y^2}\right)\left(\frac{\partial a(y)}{\partial y}\right)^2\Bigg]\Bigg]dy. \end{aligned} \tag{12}$$

In Equation (12), the crack length $a(y)$, which corresponds to crack front shape, varies along the y axis. In order to proceed, we must determine the function defining $a(y)$. It is just this, the form of the crack front, which is unknown and of interest. We assume that the functional form of $a(y)$ may be expressed as a polynomial. Allowing for symmetry with respect to the x axis and letting a_0 represent the crack length at the plate edges ($y = \pm b/2$), it is reasonable to

assume the following form:

$$a(y) = a_0 + \sum_{k=1}^{N} a_k \left[1 - \left(\frac{y}{b/2} \right)^{2k} \right]. \tag{13}$$

Since the calculation is of considerable complexity in the general case of a series of $N+1$ terms, we have restricted it to the case of $N=1$ in the present case, *i.e.*, it is assumed that the crack front is parabolic.

Equation (13) is inserted into Equation (12) and the free energy of the plate evaluated over the range $y = \pm b/2$ by numerical integration. This was achieved by using a Gauss-Newton procedure with 12 points [31]. The kinematics is given by using the beam hypothesis with length, $a(y)$, varying along the y direction.

An example of such numerical integration is presented in Figure 3. In this case, it is assumed that the (flexible) material is steel, of Young's modulus, $E = 200\,\text{GPa}$, and Poisson's ratio, $\nu = 0.3$. (In fact, E only appears in the pre-factor D and, therefore, changes nothing in the overall conformation. Poisson's ratio, ν, is, however, significant and directly related to anticlastic effects.) Plate thickness, h, is taken as 1.5 mm, width, b, as 2.5 cm, wedge thickness, Δ, as 1 mm, and a_i, the initially constant crack, or free plate, length, as 30 mm.

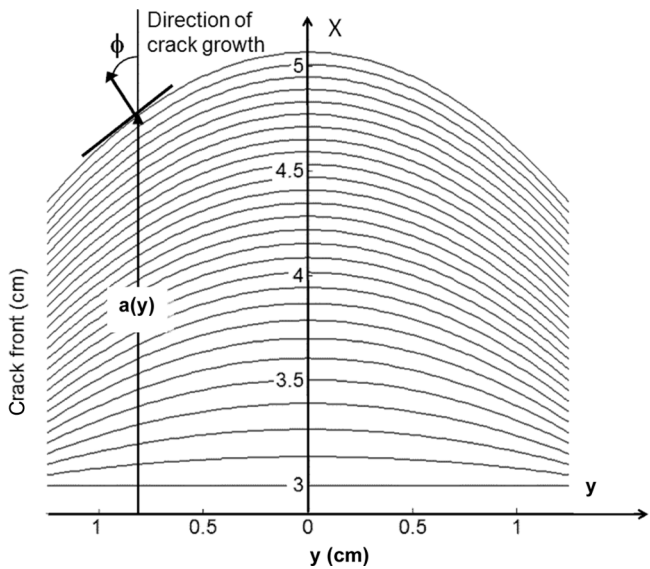

FIGURE 3 Result of numerical evaluation of Equations (12) and (13) showing crack front shape as estimated from the Kirchhoff-Love plate theory. Each line corresponds to a position of the crack front as propagation continues.

The series of curves progressing upwards from the initial horizontal line at a_i represent the iterations simulating crack growth. The aspect ratio, or "depth", of the crack-front continues to increase, which is unrealistic physically: we shall comment on this below. However, it can be clearly seen that we obtain a concave crack front with respect to the separated side of the assembly. This concavity is qualitatively in agreement with experimental observations, such as that shown in Figure 1.

Figure 3 may be compared with Figure 4, which is a 3D representation of the same scenario as described above, but achieved using finite element analysis (FEA). In order not to digress from the essential theme of this article, details of the FEA technique employed will be presented elsewhere. However, briefly, the finite element simulation considers the same boundary conditions, *i.e.*, clamped edge at the crack front, the adhesive layer is taken as perfectly rigid, the sides are supposed free, and finally, a constant displacement is applied. The FEA model enables us to take into account the anticlastic effect that might be omitted with the simple beam model. The purpose of the FEA model is to check if the strong hypothesis on the displacement field does not produce a large error in the estimate of the stressed structure energy and, consequently, in the energy released rate.

In Figure 5, we compare the two approaches directly. Using the same data as above, we present on the right hand side the progression of the crack front as evaluated by the semi-analytic approach and, on the left hand side, the progression as found using FEA. Equivalent crack lengths, as calculated at $y = \pm b/2$, are shown. It can be seen quite clearly that, for a given crack length at the edge, the two approaches lead to very similar results. At this stage, root rotation and deflection effects [28,29] have been neglected for both types of calculation to facilitate comparison. These will be taken into account in a later article.

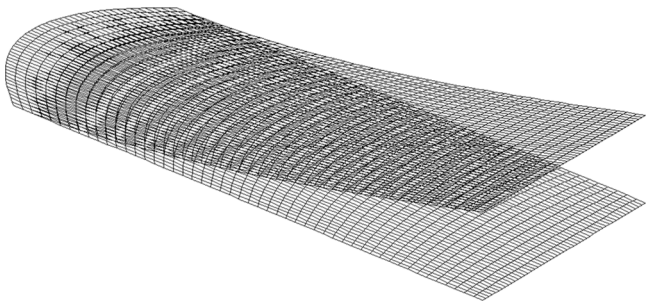

FIGURE 4 3D view of crack simulation obtained from finite element analysis.

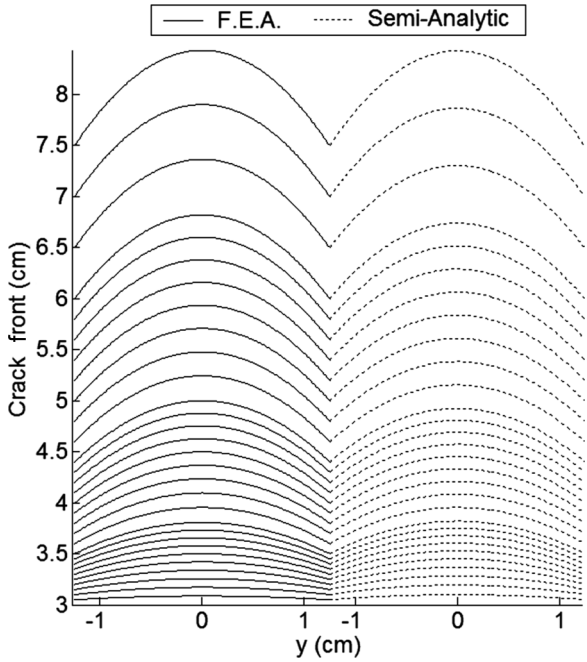

FIGURE 5 Crack propagation simulation with parabolic profile approximation: comparison between FEA (left) and semi-analytic (right) calculations, showing a good agreement between both methods.

EVALUATION OF FRACTURE ENERGY

In the plate analysis, the complete problem of evaluation of stored strain energy represented by W, which is necessary for the evaluation of strain energy release rate, G, and, therefore, fracture energy, G_c, is complex. However, to a first approximation, and notwithstanding the higher concentration of strain energy nearer the crack-front due to increased principal moment (given by Fx), Equation (12) may be used to evaluate W, assuming a *straight* crack-front and, therefore, a crack of length a_0, independent of y [corresponding to $N = 0$ in Equation (13)]. After integration, we obtain:

$$W \approx \frac{E\Delta^2 bh^3}{8a_0^3(1-\nu^2)}, \tag{14}$$

which is the same expression as that given by Equation (4), apart from the factor of $(1-\nu^2)^{-1}$, and, thus, corresponds to the simple analysis of a *wide* (or short) beam.

A more complete appraisal requires numerical integration of Equation (12). This has been carried out assuming, in this case, a

parabolic crack front [*cf.* Equation (13) with $N=1$]. The value of energy, W, thus found is presented in Figure 6 as a function of crack length (at $y=\pm b/2$), and represented by the term "semi-analytic". For comparison, we show the equivalent energy, U, from Equation (4) ("long beam"), that including a pre-factor of $(1-\nu^2)^{-1}$ ("short beam") and the finite element evaluation (F.E.A). As can be seen, for most of the range of crack length, a, studied, the simple beam analyses (long beam and short beam) somewhat overestimate strain energy, particularly the short beam, whereas the semi-analytic and FEA approaches are in good agreement. However, the order is changed slightly for crack lengths close to the initial value of 3 cm. Although the highest energy is still attributed to the short beam together with the semi-analytic model, the lowest is now that corresponding to the long beam, with the FEA in between. For long cracks, the four solutions become closer asymptotically, as strain energy tends towards zero.

Using the equation relating fracture energy, G_c, to the release of stored, strain energy, W:

$$G_c = -\frac{dW}{dS}, \tag{15}$$

where S represents surface created during fracture, we obtain, for $N=0$ [in Equation (13)]:

$$G_c = \frac{3E\Delta^2 h^3}{8a^4(1-\nu^2)}. \tag{16}$$

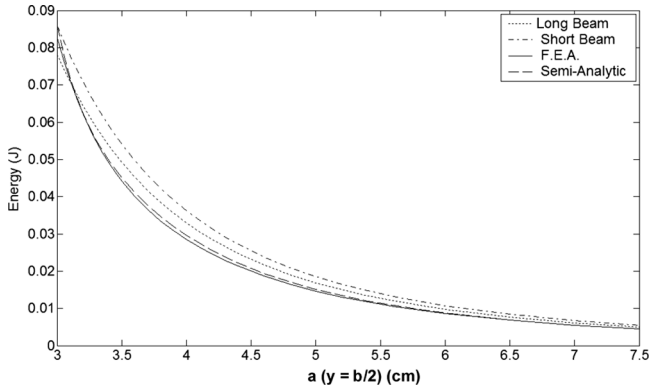

FIGURE 6 Stored elastic energy, W or U, in the separated beam as a function of crack length, a, the latter evaluated at $y=\pm b/2$. Comparison is made between the simple long beam and short beam (with pre-factor $(1-\nu^2)^{-1}$) models (both without crack front curvature), the finite element (FEA), and semi-analytic (semi-analytic) calculations.

The result given By Equation (16) was, in fact, anticipated following Equation (6) above, when allowing for a wide, or short, beam. Numerical integration for the parabolic crack front ($N = 1$) has also been done, and the resulting curve of strain energy release rate, G (corresponding to G_c in an adhesion test), *vs* a (at $y = \pm b/2$) is presented in Figure 7 (semi-analytic). In Figure 7 are also presented the results corresponding to the simple long beam and short beam models, and to the FEA analysis. In fact, the *numerical* calculation of G was effected using the assumption that the local crack propagation direction is that which, overall, reduces the strain energy, W, the most rapidly. The results show a similar trend to those portrayed in Figure 6, with the simple long beam and short beam models presenting a somewhat higher value of G over most of the range of a considered. For short cracks, *viz.* only slightly longer than the (imposed, arbitrary) initial configuration with a straight crack front at 3 cm from the wedge, in fact it is the semi-analytic solution that presents the value of highest G.

For reasons of computational complexity, we have restricted semi-analytic and FEA solutions to those corresponding to a parabolic crack front for comparison. This should be reasonably valid for relatively narrow adherends (*i.e.*, $b/a << 1$), but further terms in the series will undoubtedly be advantageous for a better approximation in the case of wide beams. Clearly, in principle, Equation (13) would permit a more refined evaluation both of stored, strain energy and energy release rate, by increasing the value of N.

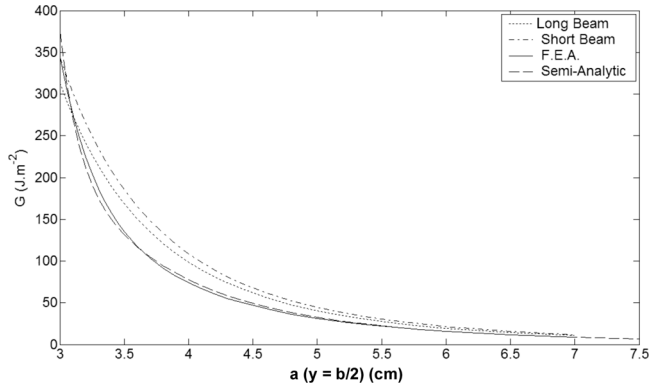

FIGURE 7 Energy release rate, G, as a function of crack length, a, the latter evaluated at $y = \pm b/2$. Comparison is made between the simple long beam and short beam [with pre-factor $(1 - \nu^2)^{-1}$] models (both without crack front curvature), the finite element (FEA), and semi-analytic (semi-analytic) calculations.

Whilst discussing fracture energy, it is instructive to compare Equation (16) with the earlier model, which assumed anticlastic bending directly [23]. In the elementary analysis of the wedge test, the adhesive fracture energy, G_c, is obtained by equating this quantity to the rate of energy release which is a function of x and, therefore, a [see Equations (4) to (6)]. In the 3D version, the principle is, of course, the same, but we must also allow for elastic energy associated with curvature in the y direction. Although this effect was taken into account for the shape of the separated beam and crack length, it was overlooked in the earlier paper as far as fracture energy is concerned [23]. Using beam theory and invoking anticlastic bending in a straightforward manner, we may assimilate the transverse bending (direction y) to a moment $m(y) = -\nu M(x)$ and curvature $w_{yy} = -\nu w_{xx}$. The supplementary strain energy is then:

$$u = \frac{2}{b}\int_0^a\int_0^{b/2} \frac{m(y)}{2} w_{yy}\, dydx = \nu^2 U. \tag{17}$$

Equation (17) may be compared directly with Equation (4). The total strain energy, U_T, can then be expressed as:

$$U_T = U + u = (1+\nu^2)U = \frac{E\Delta^2 b h^3 (1+\nu^2)}{8a_0^3}. \tag{18}$$

Using Equation (18) with Equation (5) [or (15)], we obtain, as a modified form of Equation (6):

$$G_c = \frac{3E\Delta^2 h^3 (1+\nu^2)}{8a^4}, \tag{19}$$

which, upon recognising the limited development, $(1-\nu^2)^{-1} \approx (1+\nu^2)$, is very close to the value for G_c obtained from the more detailed treatment [Equations (16)].

There is no significant difference between the two approaches, Equations (16) and (19) giving virtually identical values for fracture energy. Different simplifying assumptions have been used for the two cases, but they lead to essentially the same expression for adhesion energy. However, we must emphasise that, in both cases, the fine structure near the crack front has been ignored, and this can be important in practice, as demonstrated in both Figures 6 and 7.

DISCUSSION

There is excellent quantitative agreement between the results obtained with the semi-analytic and finite element analyses, especially

given the limitations of the semi-analytic model. The curvature is concave with respect to the direction of crack propagation. An intriguing aspect of *both* of the analyses is that an initially straight crack front develops *continuously* increasing curvature as the crack progresses. This seems to be in contradiction with (our) experimental observations, in which a fairly constant curvature is attained after initial growth from the straight starter crack. This is reasonably clear in Figure 1. However, the analyses presented here are based uniquely on *structural* effects. The process of minimisation of strain energy is regarded purely as a static, elastic effect. Although an increase of separation rate can either increase or decrease fracture energy, G_c, the former is more usual and would tend to fit in better with the type of experiment under consideration [23,32,33]. (Decreasing fracture energy with increasing fracture speed tends to be associated with "stick-slip" behaviour.) This is a *materials* aspect of the fracture process. In the analyses based on structure alone, no consideration is given to the fact that crack growth rate is found to be maximal at the centre ($y = 0$), and decreases with increasing $|y|$ in each direction towards the edges of the joint. The increased, dissipative, energy expenditure at higher speeds will tend to *decrease* growth rate as we approach the x axis. These two conflicting effects may possibly cancel at dynamic equilibrium. A dynamic energy balance may build up, thus moderating the rate of change of concavity of the crack front, leading to an essentially constant shape. An alternative possibility is that the *structural* aspect of the wedge geometry has not yet been fully mastered. Various effects still requiring attention include changes from plane stress to plane strain across the beam width, stress reduction due to the stiffness of the joint edges, and effects of elastic foundation [28,29].

This leads us to another consideration. We may ask if the direction of crack propagation plays a significant role, irrespective of accentuating curvature. With a curved crack front, the fracture process only *strictly* follows the x direction at $y = 0$. Anywhere else, the direction of crack growth is at an angle, $\phi = \tan^{-1}(-da(y)/dy) \neq 0$, to the x axis, *i.e.*, with respect to the overall direction of separation (see Figure 3). This will have an effect on crack propagation rate in the *local* principal direction: it will decrease as ϕ increases. We, therefore, raise the question of whether G_c should be considered as a *local* or as a *global* property, the latter being averaged over the width of the joint. To explain, if the joint were to consist of a large number of parallel, *independent*, thin strip beams along the y direction, each of length $a(y)$, with different values of y, each would behave in fracture according to its own, *local*, value of bending moment, function of a. However,

since the strips are in reality joined laterally, and therefore constrained, the overall fracture front will correspond to some kind of averaging of the local effects over total joint width, b, leading to a global value of G_c. This phenomenon will be directly related to the crack front curvature, even if constant: any increase in curvature, as discussed above, will only accentuate the effect. In addition, although the fracture energy, G_c, is assessed from the *area* separated during the fracture process, energy dissipation occurs at what is essentially a fracture *line*, at any given moment. With a curved fracture front, the length of the fracture front becomes $\int_{-b/2}^{+b/2}[1 + (da/dy)^2]^{1/2}\,dy > b$, and thus overall energy consumption will be greater. This does not affect the overall surface detached, but non-rectilinear propagation means that the separation occurs at a range of rates.

It should also be pointed out that, in the semi-analytical analysis, the displacement field and, therefore, the strain energy evaluation, have been approximated. This may have some influence on the final form calculated for the crack front, but since the finite element analysis leads to very similar findings, this is not thought to be a major source of error.

The above ignores root rotation effects [28,29], which can be important for the assessment of both beam shape and fracture energy. These will be discussed in a future article.

CONCLUSION

The wedge test is a useful technique for the evaluation of adhesive fracture energy. Although the test is usually considered to be an essentially two-dimensional geometry, modelled as a beam, and results, therefore, being independent of joint width, there is good reason to believe that this simplification is not always acceptable. Some of our results, and those in the literature, show that a curved crack front can result. By considering the separated adherend as a plate rather than a beam, curvature perpendicular to the principal bending can be shown to arise. Using the principle of minimal strain energy as a criterion for plate shape, equations are derived to describe adherend shape. By employing a form of perturbation theory, approximate expressions are obtained for crack front shape and strain energy. Values of the latter, compared with those obtained from the beam model, can be significantly greater. The calculations, in agreement with finite element analysis, suggest that the curvature of the crack front becomes increasingly greater as the crack progresses, but our analysis considers only *structural* properties. *Material* properties may also be important and may need to be taken

into account in order to obtain a more exact appraisal of dynamic crack shape. We discuss the relevance of the concept of local and global failure criteria.

REFERENCES

[1] Mostovoy, S. and Ripling, E. J., *J. Appl. Polym. Sci.* **10**, 351–371 (1966).
[2] Wiederhorn, S. M., Shorb, A. M., and Moses, R. L., *J. Appl. Phys.* **39**, 1569–1572 (1968).
[3] Mostovoy, S. and Ripling, E. J., *J. Appl. Polym. Sci.* **13**, 1083–1111 (1969).
[4] Kanninen, M. F., *Int. J. Fract.* **10**, 415–430 (1974).
[5] Kollek, H., *Int. J. Adhes. Adhes.* **5**, 75–80 (1985).
[6] Whitney, J. M., *Comp. Sci. Tech.* **23**, 201– 213 (1985).
[7] Cognard, J., *J. Adhes.* **20**, 1–13 (1986).
[8] Jethwa, J. K. and Kinloch, A. J., *J. Adhesion* **61**, 71–95 (1997).
[9] Blackman, B., Dear, J. P., Kinloch, A. J., and Osiyemi, S., *J. Mat. Sci. Lett.* **10**, 253–256 (1991).
[10] Meiller, M., Roche, A. A., and Sautereau, H., *J. Adhes. Sci. Tech.* **13**, 773–788 (1999).
[11] Sener, J. Y., Ferracin, T., Caussin, L., and Delannay, F., *Int. J. Adhes. Adhes.* **22**, 129–137 (2002).
[12] Cognard, J., in *Science et technologies du collage*, (Presses Polytechniques et Universitaires Romandes, Lausanne, 2000).
[13] Davidson, B. D. and Shapery, R. A., *J. Comp. Mat.* **22**, 640–656 (1988).
[14] Davy, G., Hashem, S., and Kinloch, A. J., *Int. J. Adhes. Adhes.* **9**, 69–76 (1989).
[15] Liechti, K. M. and Chai, Y. S., *Trans. ASME* **58**, 680–687 (1991).
[16] Sutton, M. A., Dawicke, D. S., and Newman, Jr. J. C., *Fract. Mech.* **26**, 243–255 (1995).
[17] Bader, M. G., Hamerton, I., Hay, J. N., Kemp, M., and Winchester, S., *Composites A* **31**, 603–608 (2000).
[18] Imanaka, M., Takeguchi, Y., Nakamure, Y., Nishimura, A., and Iida, T., *Int. J. Adhes. Adhes.* **21**, 389–396 (2001).
[19] Chen, B., Dillard, D. A., Dillard, J. G., and Clark, R. L., *J. Adhesion* **75**, 405–434 (2001).
[20] Al-Khanbashi, A., Petiau, C., Hamdy, A. E., and Moet, A., *J. Adhes. Sci. Tech.* **17**, 1093–1107 (2003).
[21] Zhang, S., Panat, R., and Hsia, K. J., *J. Adhes. Sci. Tech.* **13**, 1685–1711 (2003).
[22] Qi, J. and Dillard, D. A., *J. Adhesion* **79**, 559–579 (2003).
[23] Popineau, S., Gautier, B., Slangen, P., and Shanahan, M. E. R., *J. Adhesion* **80**, 1173–1194 (2004).
[24] Kuhn, H. and Medlin, D. (Eds.) *ASM Handbook*, (ASM International, Metals Park, OH, 2000), Vol. 8, pp. 109–110.
[25] Krasucki, F., Münch, A., and Ousset, Y., *Inter J. Solids Structures* **39**, 6355–6383 (2002).
[26] Timonshenko, S. P. and Goodier, J. N. *Theory of Elasticity*, (McGraw-Hill, New York, 1970), 3rd ed.
[27] Williams, J. G., in *Fracture Mechanics of Polymers*, (Ellis Horwood, Chichester, 1984).
[28] Kanninen, M. F., *Int. J. of Fracture* **9**, 83–92 (1973).
[29] Sargent, J. P., *Int. J. Adhes. Adhes.* **25**, 247–256 (2005).

[30] Timoshenko, S. P. and Woinowsky-Krieger, S., in *Theory of Plates and Shells*, (McGraw-Hill, New York, 1959).
[31] Abramovitz, M. and Stegun, I. A. (Eds.) in *Handbook of Mathematical Functions* (*with Formulas, Graphs, and Mathematical Tables*, (Dover, New York, 1972).
[32] Ferry, J. D., in *Viscoelastic Properties of Polymers*, (Wiley, New York, 1970), 2nd ed.
[33] Gent, A. N. and Petrich, R. P., *Proc. Roy. Soc. London Ser. A* **310**, 433–448 (1969).